Applied Catalysis B: Environmental 252 (2019) 222–229

Contents lists available at ScienceDirect

Applied Catalysis B: Environmental

journal homepage: www.elsevier.com/locate/apcatb

Z-scheme water splitting by microspherical Rh-doped $SrTiO_3$ photocatalysts prepared by a spray drying method

Hong Phong Duong[a], Takahiro Mashiyama[a], Makoto Kobayashi[a,1], Akihide Iwase[b,c], Akihiko Kudo[b,c], Yusuke Asakura[a], Shu Yin[a], Masato Kakihana[a], Hideki Kato[a,*]

[a] Institute of Multidisciplinary Research for Advanced Materials, Tohoku University, 2-1-1 Katahira, Aoba-ku, Sendai, Miyagi, 980-8577, Japan
[b] Department of Applied Chemistry, Faculty of Science, Tokyo University of Science, 1-3 Kagurazaka, Shinjuku-ku, Tokyo, 162-8501, Japan
[c] Photocatalysis International Research Center, Research Institute for Science and Technology, Tokyo University of Science, 2641 Yamazaki, Noda-shi, Chiba, 278-8510, Japan

ARTICLE INFO

Keywords:
Photocatalyst
Water splitting
Visible light
Electron mediator
Dispersibility

ABSTRACT

Microspherical particles of Rh-doped $SrTiO_3$ ($SrTiO_3$:Rh) having size of 1–2 μm were synthesized by a spray drying (SD) method employing a water-soluble ammonium trilactatotitanate. When the calcination temperature increased up to 1200 °C, primary particles grew significantly while the microspherical morphology of the secondary particles was kept. Dynamic light scattering analysis proved well-dispersive nature of the SD sample. Photocatalytic activities of $SrTiO_3$:Rh synthesized by the SD method, solid state reaction (SSR), and a polymerizable complex (PC) method were evaluated for H_2 evolution using an electron donor such as methanol, Fe^{2+}, or $[Co(bpy)_3]^{2+}$ and Z-scheme water splitting combined with $BiVO_4$ of an O_2-evolving photocatalyst and either $Fe^{3+/2+}$, $[Co(bpy)_3]^{3+/2+}$, or reduced graphene oxide as an electron mediator. $SrTiO_3$:Rh prepared by the SD method showed much higher activities for all Z-scheme water splitting than the samples synthesized by the SSR method. Activities of the SD sample for Z-scheme water splitting using electron shuttles, $Fe^{3+/2+}$ and $[Co(bpy)_3]^{3+/2+}$, were slightly higher or comparable to those of the PC sample whereas the SD sample achieved higher activity in Z-scheme water splitting based on interparticle electron transfer. In addition, even when the mass of $SrTiO_3$:Rh used for the Z-scheme system with $Fe^{3+/2+}$ was decreased from 50 mg to 30 mg, the SD sample still showed high activity while the activity decreased for the SSR and PC samples. Thus, usefulness of the SD method to obtain highly active $SrTiO_3$:Rh with well-dispersive nature has been demonstrated.

1. Introduction

Conversion of solar energy to H_2 via water splitting is known as a promising solution for energy and global warming issues [1]. Photocatalytic water splitting is one of the candidates for solar H_2 production and is extensively studied [2–8]. Great efforts have been mobilized to design 2-step photoexcitation systems composed of two kinds of photocatalysts, which are generally called as Z-scheme systems, because the Z-scheme systems are able to achieve overall water splitting despite that the photocatalysts used in the Z-scheme systems are inactive for overall water splitting themselves [9–27]. Rh-doped $SrTiO_3$, denoted as $SrTiO_3$:Rh hereafter, is a highly active visible-light-driven photocatalyst for H_2 evolution in the presence of electron donors [28] and is useful as a H_2-evolving photocatalyst in Z-scheme systems based on electron shuttle reagents such as $Fe^{3+/2+}$, $Co^{3+/2+}$-complexes, and $[Fe(CN)_6]^{3-/4-}$ [10,13,15–18,20], interparticle electron transfer [12,14,19], and electron conductive layers [22]. In a typical Z-scheme system, $SrTiO_3$:Rh is combined with a suitable O_2-evolving photocatalyst such as $BiVO_4$ and a redox electron shuttle such as $Fe^{3+/2+}$ [10,15], and $Co^{3+/2+}$-complexes [16], in which photogenerated electrons in $SrTiO_3$:Rh and photogenerated holes in $BiVO_4$ are used for reduction of protons and oxidation of H_2O molecules to form H_2 and O_2, respectively. The redox electron shuttle transfers electrons in conduction band of $BiVO_4$ to $SrTiO_3$:Rh, thus holes in Rh^{3+} level of $SrTiO_3$:Rh are eliminated. On the other hand, even without any redox electron shuttle, Z-scheme overall water splitting can also be achieved by interparticle electron transfer, in which the photogenerated carriers are transferred by physical contact between $SrTiO_3$:Rh and $BiVO_4$ [12,14,19] and reduced graphene oxide (denoted as RGO) deposited on $BiVO_4$ can facilitate the interparticle electron transfer [14]. These Z-

* Corresponding author.
E-mail address: hideki.kato.e2@tohoku.ac.jp (H. Kato).
[1] Present address: Institute of Materials and Systems for Sustainability, Nagoya University, Furo-cho, Chikusa-ku, Nagoya 464-8601, Japan.

https://doi.org/10.1016/j.apcatb.2019.04.009
Received 16 December 2018; Received in revised form 2 April 2019; Accepted 6 April 2019
Available online 18 April 2019
0926-3373/

scheme systems have been established with use of $SrTiO_3$:Rh synthesized by a conventional solid state reaction (SSR) method. Improvement of activity of the component photocatalysts is indispensable to realize an efficient Z-scheme system, thus many attempts especially synthesis using solution based methods have been focused in order to enhance the activity of $SrTiO_3$:Rh [10,15,29]. The present authors have reported that the reactivity of $SrTiO_3$:Rh is varied by the synthetic routes and that the activity of Z-scheme system using an $Fe^{3+/2+}$ electron shuttle is improved when $SrTiO_3$:Rh powders prepared by polymerizable complex (PC) and hydrothermal (HT) methods are employed [15]. However, there are no reports on improvements of activities of Z-scheme systems composed of $SrTiO_3$:Rh and $BiVO_4$ with $Co^{3+/2+}$-complexes or RGO, although these systems have an advantage against the system using $Fe^{3+/2+}$. The reactant solution of the Z-scheme system using $Fe^{3+/2+}$ should be acidic (pH $<$ 2.5) to avoid hydrolysis of iron ions, while the Z-scheme systems using $Co^{3+/2+}$-complexes or RGO are basically available in wide pH ranges [10,14,16]. In addition, $SrTiO_3$:Rh prepared by the PC method is comprised of large agglomerations of several tens micrometers in spite of fine primary particles, being a negative factor in dispersibility of the sample [15]. It is known that higher dispersion of photocatalysts gives the higher photocatalytic activity [30–32]. Therefore, a novel $SrTiO_3$:Rh photocatalyst possessing well-dispersive nature and high activity is demanded for the development of the Z-scheme systems.

A spray drying (SD) method is a useful solution-based synthetic route to obtain microspherical particles [33–36]. Hence, it is expected that highly active $SrTiO_3$:Rh powder can be obtained by the SD method offering an advantage of well-dispersive microspherical particles in addition to homogeneous distribution of constituent elements although no one has demonstrated the synthesis of $SrTiO_3$:Rh by the SD method. Alkoxides and chloride of titanium, which are frequently used as Ti-sources for solution-based synthesis, are not suitable Ti-sources for the SD method due to a risk of explosion of organic solvent required for usage of alkoxides or corrosion of the SD apparatus by strong acid in usage of titanium chloride. Kakihana et al. have reported water-soluble titanium compounds, which give very stable aqueous solutions in wide pH range [37–39]. Therefore, the water-soluble titanium compounds can be considered as suitable Ti-sources for the aqueous solution-based SD method.

In the present study, synthesis of $SrTiO_3$:Rh particles by the SD method utilizing the water-soluble titanium compound was examined for the first time. The photocatalytic activities of $SrTiO_3$:Rh prepared by SD, SSR, and PC methods for H_2 evolution using an electron donor, such as methanol, Fe^{2+}, and $[Co(bpy)_3]^{2+}$, and water splitting by Z-scheme systems combined with $BiVO_4$ and $Fe^{3+/2+}$, $[Co(bpy)_3]^{3+/2+}$, or RGO were compared to know characteristics of $SrTiO_3$:Rh prepared by different methods.

2. Experimental

2.1. Synthesis of photocatalyst powders

Powders of $SrTiO_3$:Rh with different amounts of Sr were prepared by the SD method. Powders of strontium acetate hemihydrate (Wako, 99.0%), rhodium acetate dimer dihydrate (Wako, 42.5% as Rh), and homemade ammonium trilactatotitanate, which were prepared by a manner reported in literature [37] but with some modifications (see Supplementary material for the detailed procedure), were dissolved in distilled water in a ratio Sr:Ti:Rh = 1.00 + y:0.98:0.02. Use of other water-soluble titanium compounds, such as glycolatoperoxotitanate and citratoperoxotitanate complexes, and strontium nitrate were not appropriate for the SD method. Precipitation occurred in the mixed solution when water-soluble titanium compounds other than ammonium trilactatotitanate were used. When nitrates were employed, vigorous combustion caused by ammonium nitrate and organics occurred in the pyrolysis of the dried sample, resulting in heavily sintered large particles. The concentration of the solution was 20 mM in respect of $SrTiO_3$:Rh. The mixed solution was supplied to a spray dryer apparatus (Yamato; ADL310) at a rate 10 mL min^{-1}. Hot air (175 °C) was also supplied to the spray dryer at 0.1 MPa of gauge pressure to make spray of the mixed solution, and then to dry it in a drying chamber of the apparatus. During this step, the starting solution was transformed into dried particles. The dried particles were then collected by a cyclone separator of the apparatus. The dried powder thus obtained was immediately subjected to pyrolysis in air, in which the sample was put in a mantle heater at 200 °C with gradual increases in temperature with 50 °C of step up to 450 °C to obtain a precursor powder. Finally, the precursor was calcined at 900–1200 °C for 10 h in air using an alumina crucible. The powders of $SrTiO_3$:Rh were also prepared by SSR and PC methods for comparison. Amounts of Rh doped were at 1 and 2 mol% for the SSR and PC samples, respectively, according to the literature [15]. The $SrTiO_3$:Rh samples prepared by SD, SSR, and PC methods are denoted as SD-Y%, SSR-Y%, and PC-Y%, respectively, where Y indicates percentage of excessive Sr. Either Pt(0.3 wt%) or Ru(1 wt%) was deposited on $SrTiO_3$:Rh as a cocatalyst for H_2 evolution by a photoreduction method in an aqueous methanol solution (10 vol%) containing an intended amount of H_2PtCl_6 or $RuCl_3$ [15].

$BiVO_4$ powder used as an O_2-evolving photocatalyst in Z-scheme systems was synthesized by a liquid-solid reaction from bismuth nitrate pentahydrate (Kanto, 99.5%) and $K_3V_5O_{14}$ [40]. For Z-scheme water splitting based on interparticle electron transfer, $BiVO_4$ modified with 5 wt% of RGO (RGO/$BiVO_4$) was prepared by a photoreduction method [14].

2.2. Characterization of photocatalysts

The crystal phases of samples were characterized by X-ray diffraction utilizing Cu Kα radiation (XRD; Bruker AXS, D2 Phaser). Reflectance spectra of samples were measured by an ultraviolet-visible spectrometer (UV–vis; Shimadzu, UV-3100) equipped with an integrating sphere and were converted by the Kubelka-Munk method. Particle size distribution of samples in suspensions of 2-propanol (Kanto, 99.7%) with 0.2 wt% of $SrTiO_3$:Rh was analyzed by a dynamic light scattering method (DLS; Malvern, Zetasizer Nano ZS). Surface elemental composition was analyzed by X-ray photoelectron spectroscopy (XPS; Kratos, ESCA-3400) using Mg Kα as an excitation source. Sample observation was performed using scanning electron microscopes (SEM; Hitachi, SU1510 and Jeol, JSM-6700 F). Specific surface areas (S_{BET}) were determined by the Brunauer-Emmett-Teller method based on N_2 adsorption at 77 K (MicrotracBEL; BELSORP-miniII). Adsorption of iron ions on samples was examined in the dark. 0.3 g of $SrTiO_3$:Rh powder was put into a 20 mL solution containing either 2 mM of $FeSO_4$ or 1 mM of $Fe_2(SO_4)_3$ at pH 2.1, which was prepared from sulfuric acid (Wako, 95%) and $FeSO_4{\cdot}7H_2O$ (Wako, 99.5%) or $Fe_2(SO_4)_3{\cdot}nH_2O$ (Wako, 99.5%). After 5 h of stirring, supernatant solution was collected by a centrifugal method. The concentrations of Fe^{2+} and Fe^{3+} in the supernatant solution were determined by a colorimetric method based on a 1,10-phenanthroline-iron(II) complex as reported elsewhere [10].

2.3. Photocatalytic reactions

H_2 evolution and Z-scheme water splitting reactions were examined to evaluate performance of $SrTiO_3$:Rh photocatalysts obtained with different conditions. For H_2 evolution, methanol (Kanto, 99.8%), Fe^{2+} and $[Co(bpy)_3]^{2+}$ were employed as electron donors with concentration of 10 vol%, 5 mM, and 2 mM, respectively. $FeSO_4{\cdot}7H_2O$ was used as an Fe^{2+} source whereas $[Co(bpy)_3]SO_4$ was synthesized by mixing $CoSO_4{\cdot}7H_2O$ (Kanto, 99.0%) and 2,2′-bipyridine (Kanto, 99.5%) at stoichiometric ratio in a 75 vol% aqueous ethanol solution [16]. Sulfuric acid (Wako, 95%) was used to adjust pH of $FeSO_4$ and $[Co(bpy)_3]SO_4$ solutions at 2.4 and 3.8, respectively. The Pt cocatalyst was used

for H_2 evolution using methanol while the Ru cocatalyst was used for other reactions. Three kinds of systems using either $Fe^{3+/2+}$, $[Co(bpy)_3]^{3+/2+}$, or RGO as the electron mediator were examined for Z-scheme water splitting utilizing $Ru/SrTiO_3$:Rh and $BiVO_4$. As reactant solutions, 1 mM of $Fe_2(SO_4)_3$ at pH 2.4, 0.5 mM of $[Co(bpy)_3]SO_4$ at pH 3.8, and sulfuric acid solution at pH 3.5 were used. These pH values were reported as optimal ones [10,14,16]. All photocatalytic reactions were conducted in a gas-closed circulation system with a 300 W Xe-arc lamp (Excelitas, Cermax PE300BF). Visible light ($\lambda > 420$ nm) was used for typical reactions but monochromatic light at 420 nm extracted by an interference filter (Kenko, BP-42) was used for evaluation of apparent quantum yields (AQY). A solar simulator with 100 mW cm^{-2} of incident density (Asahi spectra, HAL-320) was also used to evaluate efficiency of solar energy conversion to hydrogen (STH). Amounts of photocatalysts used were 30–100 mg for H_2 evolution, and 20–50 mg of $Ru/SrTiO_3$:Rh and 50 mg of $BiVO_4$ for Z-scheme water splitting. Temperature of the reactant solution was maintained at 20 °C using a water bath during photocatalytic reactions. An on-line gas chromatograph (Shimadzu, GC-8 A, TCD, Ar carrier, MS-5 A column) was employed to determine the amounts of generated H_2 and O_2.

3. Results and discussion

3.1. $SrTiO_3$:Rh prepared by SD method

XRD patterns of SD-5% calcined at various temperatures are shown in Fig. 1. The dried powder collected by the spray dryer was amorphous while the precursor crystallized in a $SrTiO_3$ phase without any impurities. Crystallinity was increased as the calcination temperature became higher. It should be noticed that the direct formation of the target phase without formation of impurities, such as TiO_2, $SrCO_3$, and other strontium titanates, indicates homogeneous distribution of constituent elements in the powder obtained by the present spray drying method as well as the PC method [41]. XRD patterns of samples prepared by different methods with calcination at 1100 °C are compared in Fig. S1, where SD-5%, SSR-3%, and PC-3%, which have the highest activity for each method as described later, are compared. A remarkable difference can be seen between SSR-3% and samples prepared by solution based methods (SD-5% and PC-3%) in terms of phase purity. Although the presence of layered perovskite structure is obviously seen as a small extra peak at lower angle side of the main peak for SSR-3%, such an extra diffraction peak is not present in SD-5% and PC-3%. The formation of Sr-rich layered perovskite structure with only 3 mol% of excessive Sr is due to low homogeneity in the SSR sample [15]. XRD patterns of the SD samples calcined at 1100 °C with different amounts

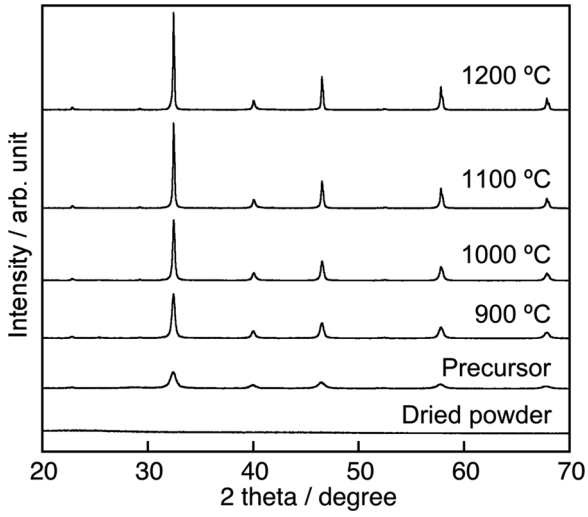

Fig. 1. XRD patterns of SD-5% calcined at various temperatures for 10 h.

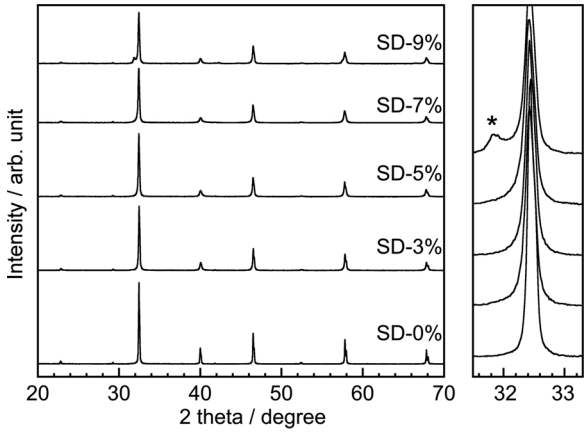

Fig. 2. XRD patterns of SD samples calcined at 1100 °C for 10 h with different amounts of excessive Sr.

of excessive Sr are shown in Fig. 2. The SD samples with 0–7 mol% of excessive Sr were ascribed to pure phase of $SrTiO_3$ while the diffraction peaks owing to layered perovskite structure showed up in SD-9%. The appearance of the layered perovskite structure in samples prepared by solution-based method with ca. 10 mol% of excessive Sr is consistent with the previous result [15].

Morphological properties are important for the SD samples taking consideration of the aim of this research, that is, development of a new synthetic route offering advantages of high homogeneity of constituents and good dispersibility. Fig. 3 presents SEM images of SD-5% calcined at 900–1200 °C, and Table 1 summarizes S_{BET} and sizes of primary particles. Secondary particles in the precursor had spherical morphology with size of 1–2 μm, which was composed of very fine primary particles (around 10 nm) and gave large S_{BET}, 40.7 $m^2 g^{-1}$. As the calcination temperature increased from 900 °C to 1200 °C, the primary particles remarkably grew from 30 to 500 nm in sizes. Accordingly, S_{BET} of SD-5% decreased to 18.5, 7.6, 2.5, and 0.9 $m^2 g^{-1}$ with increases in the calcination temperature. Nevertheless, the secondary particles of the SD sample retained spherical morphologyeven after calcination at 1100 and 1200 °C (Figs. 3 and S2). The sizes of primary particles in SD-5% calcined at 1100 °C were similar to those in PC-3% and were slightly smaller than those in SSR-3%, while the secondary particles of SD-5% (1–2 μm) were significantly smaller than those of PC-3% (1–30 μm) as shown in Fig. S2. Fig. 4 shows particle size distribution of SD-5%, SSR-3%, and PC-3% calcined at 1100 °C. SD-5% gave sharp distribution peaking around 1 μm in good agreement with the secondary particle sizes observed by SEM. PC-3% also showed strong distribution around 1 μm, however, it had portions at larger sizes. Moreover, a large number of particles sank in the PC-3% suspension within 1 min after shaking as shown in Fig. S3. From these facts, it is obvious the presence of larger particles in PC-3% beyond the upper limit of the instrument (6 μm). SSR-3% basically showed distribution around 1 μm however it also had a small portion around 6 μm, indicating the presence of aggregated particles. Thus, the well dispersibility of SD-5% compared to PC-3% was clarified. S_{BET} of SD-5% (2.5 $m^2 g^{-1}$) was slightly larger than those of SSR-3% (2.4 $m^2 g^{-1}$) and PC-3% (1.7 $m^2 g^{-1}$). The amounts of excessive Sr in SD samples were less effective for morphological properties, S_{BET}, and sizes of primary particles (Table 1 and Fig. S4).

3.2. Photocatalytic activity of SD samples for Z-scheme water splitting using an $Fe^{3+/2+}$ electron shuttle

Table 2 summarizes photocatalytic activities of $SrTiO_3$:Rh samples for sacrificial H_2 evolution and Z-scheme water splitting using $Fe^{3+/2+}$, where amounts of photocatalysts were 50 mg for both $Ru/SrTiO_3$:Rh and $BiVO_4$. It should be notified that the same activity for Z-scheme water splitting can be obtained in use of $FeCl_3$ and $Fe_2(SO_4)_3$ as the

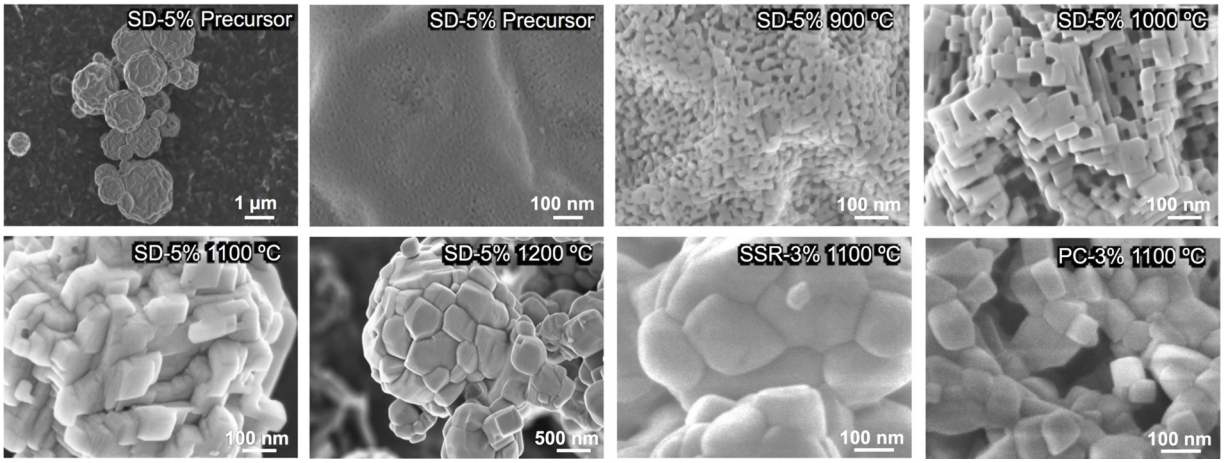

Fig. 3. SEM images of SD-5% calcined at various temperatures. SEM images of SSR-3% and PC-3% calcined at 1100 °C are also shown.

Table 1
S_{BET} and primary particle size of $SrTiO_3$:Rh.

Sample	Calcination temperature / °C	S_{BET} / $m^2\ g^{-1}$	Primary particle size / nm
SD-0%	1100	2.3	100–200
SD-3%	1100	3.2	100–150
SD-5%[a]	–	40.5	< 10
SD-5%	900	18.5	30–50
SD-5%	1000	7.6	50–100
SD-5%	1100	2.5	100–200
SD-5%	1200	0.9	500
SD-7%	1100	2.9	100–200
SD-9%	1100	3.1	200–300
SSR-3%	1100	2.4	150–200
PC-3%	1100	1.7	80–150

[a]Precursor.

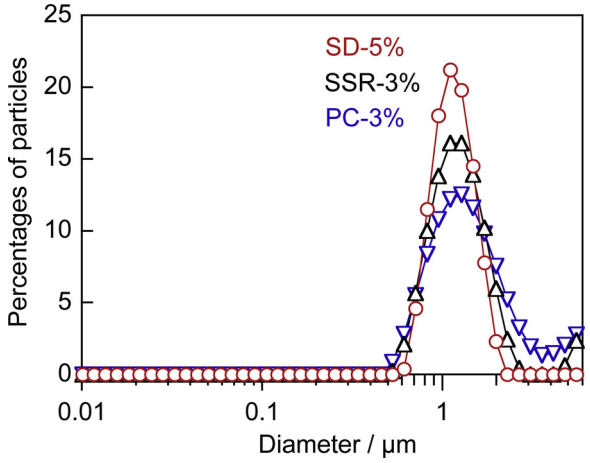

Fig. 4. Size distribution for SD-5%, SSR-3%, and PC-3% analyzed by the DLS method.

Fe^{3+} source as shown in Fig. S5 although $FeCl_3$ was reported as the best Fe^{3+} source for the Z-scheme system employing Pt/$SrTiO_3$:Rh and $BiVO_4$ [10]. It would be due to less probability of backward reaction over the Ru cocatalyst. Therefore, $Fe_2(SO_4)_3$ was used as the Fe^{3+} source in this study. The activities of SD-5% strongly depended upon the calcination temperature for both reactions. SD-5% calcined at 900 °C was inactive in Z-scheme water splitting in spite of its large S_{BET}. It has been reported that the reversible Rh^{3+} ions formed by photoreduction of Rh^{4+} ions are important to obtain high activity for $SrTiO_3$:Rh [29]. In UV–vis spectra of SD-5% calcined at 900 °C (Fig. S6),

Table 2
Activities of $SrTiO_3$:Rh for H_2 evolution using methanol and Z-scheme water splitting by the Ru(1 wt%)/STO:Rh-$BiVO_4$-$Fe^{3+/2+}$ system under visible light irradiation.

Sample	Calcination temperature / °C	Rate of evolution / μmol h^{-1}		
		H_2[a]	H_2[b]	O_2[b]
SD-0%	1100	12.5	0.5	2.0
SD-3%	1100	49.6	66.1	33.6
SD-5%	900	16.5	2.4	1.9
SD-5%	1000	51.0	33.9	16.6
SD-5%	1100	84.1	68.1	33.2
SD-5%	1200	11.0	5.0	4.2
SD-7%	1100	52.1	56.1	28.4
SD-9%	1100	77.0	49.0	24.6
SSR-2%	1100	68.1	21.3	10.1
SSR-3%	1100	103.3	35.1	16.9
SSR-5%	1100	81	34.9	17.0
PC-3%	1100	40.0	60.1	29.7
PC-5%	1100	57.7	58.5	27.8

Reaction vessel: a top-window cell, light source: 300 W Xe lamp (λ > 420 nm).
[a] For H_2 evolution from 10 vol% aqueous methanol solution (160 mL) using Pt(0.3 wt%)/$SrTiO_3$:Rh (100 mg).
[b] For water splitting in Z-scheme system employing Ru(1 wt%)/$SrTiO_3$:Rh (50 mg) and $BiVO_4$ (50 mg) in 1 mmol L^{-1} $Fe_2(SO_4)_3$ aqueous solution (160 mL) at pH 2.4.

intensity of an absorption band peaking at 570 nm attributed to electron transition from the valence band to acceptor levels formed by Rh^{4+} was weak while absorption around 420 nm ascribed to electron transition from the donor levels formed by Rh^{3+} to the conduction band was intense, meaning that Rh^{3+} was stabilized in this sample. The absorption relating to Rh^{4+} became strong when the sample was calcined at 1000 °C and higher. Thus, UV–vis spectra indicate an importance of calcination at high temperature to form appropriate amount of Rh^{4+} ions in the SD sample like $SrTiO_3$:Rh prepared by other solution based methods [15,29]. Besides, calcination at excessively high temperature (1200 °C) decreased activity due to the remarkable growth of primary particles to 500 nm. The recombination of photogenerated carriers is relatively enhanced in such large particles because the traveling distance of carriers to the surface becomes longer. The calcination at 1100 °C was suitable for the present SD method to obtain highly active samples for sacrificial H_2 evolution and Z-scheme water splitting. For SD samples calcined at 1100 °C, amounts of excessive Sr strongly affected activities. The sample without excessive Sr (SD-0%) was almost inactive while SD-3–9% showed high activity. Thus, excessive Sr is indispensable for the SD samples to obtain high activity as well as the SSR, PC, and HT samples [15]. Among the SD samples, SD-5% showed

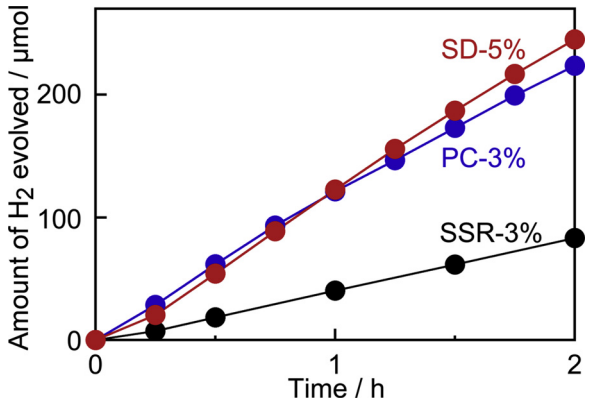

Fig. 5. H_2 evolution from an aqueous $FeSO_4$ solution over SD-5%, SSR-3%, and PC-3% modified with Ru(1 wt%). Catalyst: 30 mg, reactant solution: 160 mL of 5 mM of $FeSO_4$ at pH 2.4, light source: 300 W Xe lamp (λ > 420 nm).

Table 3
Surface properties of $SrTiO_3$:Rh.

Sample	S_{BET} / $m^2 g^{-1}$	Atomic composition[a]			Amount of adsorbed Fe / μmol g^{-1} (/ μmol m^{-2})	
		Sr	Ti	Rh	Fe^{2+}	Fe^{3+}
SD-5%	2.5	1.53	0.97	0.03	16.7 (6.7)	18.0 (7.2)
SSR-3%	2.4	1.60	0.91	0.09	8.7 (3.6)	16.7 (7.0)
PC-3%	1.7	1.43	0.97	0.03	8.7 (5.1)	12.0 (7.1)

[a] Surface atomic composition determined by XPS.

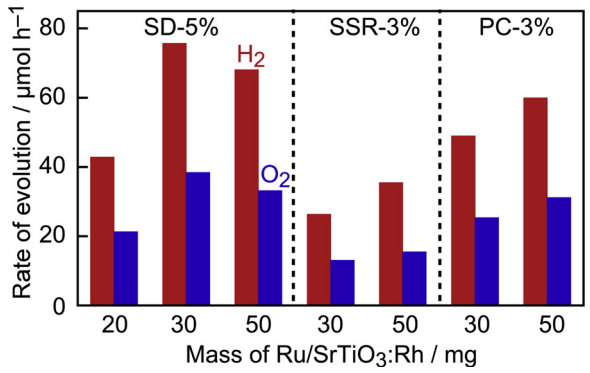

Fig. 6. Influences of amounts of Ru(1 wt%)/$SrTiO_3$:Rh on activity of the Z-scheme system composed of Ru(1 wt%)/$SrTiO_3$:Rh and $BiVO_4$. Catalysts: 20–50 mg for Ru(1 wt%)/$SrTiO_3$:Rh and 50 mg for $BiVO_4$, reactant solution: 160 mL of 1 mM $Fe_2(SO_4)_3$ at pH 2.4, light source: 300 W Xe lamp (λ > 420 nm).

the highest activity for both H_2 evolution and water splitting. Influences of amounts of excessive Sr upon activities were also examined for SSR and PC samples. For water splitting, samples with 3% excessive Sr showed the higher activity for SSR and PC methods although differences between 3% and 5% samples were very small. Therefore, photocatalytic properties of SD-5%, SSR-3%, and PC-3% samples with the highest activity for each synthetic method were further compared. SSR-3% showed a higher activity for H_2 evolution from methanol solution than others whereas SD-5% and PC-3% showed remarkably higher activity for water splitting than SSR-3%. SD-5% and PC-3% produced H_2 from an aqueous $FeSO_4$ solution at remarkably higher rates than SSR-3% (Fig. 5). Adsorption properties of iron ions on $SrTiO_3$:Rh samples are summarized in Table 3 with surface atomic composition determined by XPS. In all samples, the contents of Sr at the surface are larger than the nominal ratios and there are no significant differences among them. No difference is seen in the content of Rh between SD-5% and PC-3%

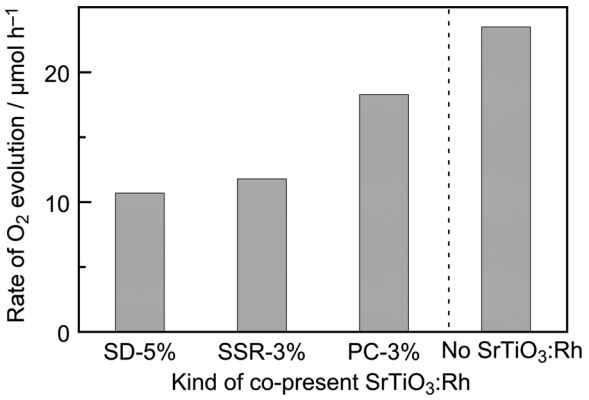

Fig. 7. Influences of co-present $SrTiO_3$:Rh upon O_2 evolution over $BiVO_4$ using Fe^{3+}. Catalysts: 50 mg for each, reactant solution: 160 mL of 1 mM $Fe_2(SO_4)_3$ at pH 2.4, light source: 300 W Xe lamp (λ > 420 nm).

while SSR-3% has a remarkably large content of Rh at the surface. This also supports the achievement of homogeneous distribution of the Rh dopant by the solution-based methods than the SSR method. When the adsorbed amount of Fe^{3+} is compared per unity of mass, it looks to depend on the synthesis method. However, the adsorbed amount of Fe^{3+} per 1 m^2 of the surface area is almost the constant at 7.1 ± 0.1 μmol m^{-2}. Thus, synthetic methods and the Rh contents give no influences upon the density of Fe^{3+} adsorbed on the surface at least in the present samples. In contrast, the affinity to Fe^{2+} in the unit of μmol m^{-2} changes in the order of SSR-3% < PC-3% < SD-5%, being roughly the same tendency as that of activity for H_2 evolution using Fe^{2+} as an electron donor. This suggests that the high activity of SD-5% and PC-3% for H_2 evolution is caused by the higher affinity to Fe^{2+} in those samples than the SSR sample. Thus, the high activity of SD-5% and PC-3% for Z-scheme water splitting is due to highly efficient H_2 evolution over Ru/$SrTiO_3$:Rh rather than other reasons such as suppression of backward reactions. However, the reasons for higher affinity to Fe^{2+} in SD-5% and PC-3% have not been clarified at this time. Next, stability of the Z-scheme system using SD-5% was examined under a long time visible light irradiation with intermittent evacuations. The rates of H_2 and O_2 evolution with ratio of 2:1 were remained stable over 54 h of irradiation as shown in Fig. S7.

The activities of the SD samples (SD-3% and SD-5%) for Z-scheme water splitting using $Fe^{3+/2+}$ were only 10–13% higher than that of PC-3% even though the SD samples had the well-dispersive nature, which was expected as an advantageous characteristic to the PC samples. The influences of the well-dispersive nature of the SD sample upon Z-scheme water splitting were further investigated by changing the amounts of Ru/$SrTiO_3$:Rh in the Z-scheme systems. Fig. 6 shows the activities of Z-scheme systems using different amounts of Ru/$SrTiO_3$:Rh (20–50 mg) and 50 mg of $BiVO_4$. When the amount of Ru/$SrTiO_3$:Rh was reduced from 50 to 30 mg, the activity of SD-5% was enhanced about 10% while those of SSR-3% and PC-3% were decreased. The dispersibility of Ru/$SrTiO_3$:Rh is responsible for the different result between SD-5% and PC-3% systems. The activities of SD-5% and PC-3% for H_2 evolution using Fe^{2+} were comparable to each other even when 30 mg of the sample was used as shown in Fig. 5. In Z-scheme systems made of suspension of both Ru/$SrTiO_3$:Rh and $BiVO_4$ particles, dispersibility of photocatalysts affects the proportion of photoexcitation of each photocatalyst. To know influences of dispersibility of $SrTiO_3$:Rh, O_2 evolution over $BiVO_4$ was examined in the presence of bare $SrTiO_3$:Rh (Fig. 7). In these experiments, H_2 evolution owing to Z-scheme water splitting was negligible because of lacking active sites (cocatalysts) for H_2 evolution, therefore rates of O_2 evolution reflected the efficiency of photoexcitation of $BiVO_4$ in the system. O_2 evolution was suppressed by addition of any kinds of $SrTiO_3$:Rh, indicating the inhibition of photoexcitation of $BiVO_4$ by $SrTiO_3$:Rh. Co-present SD-5%

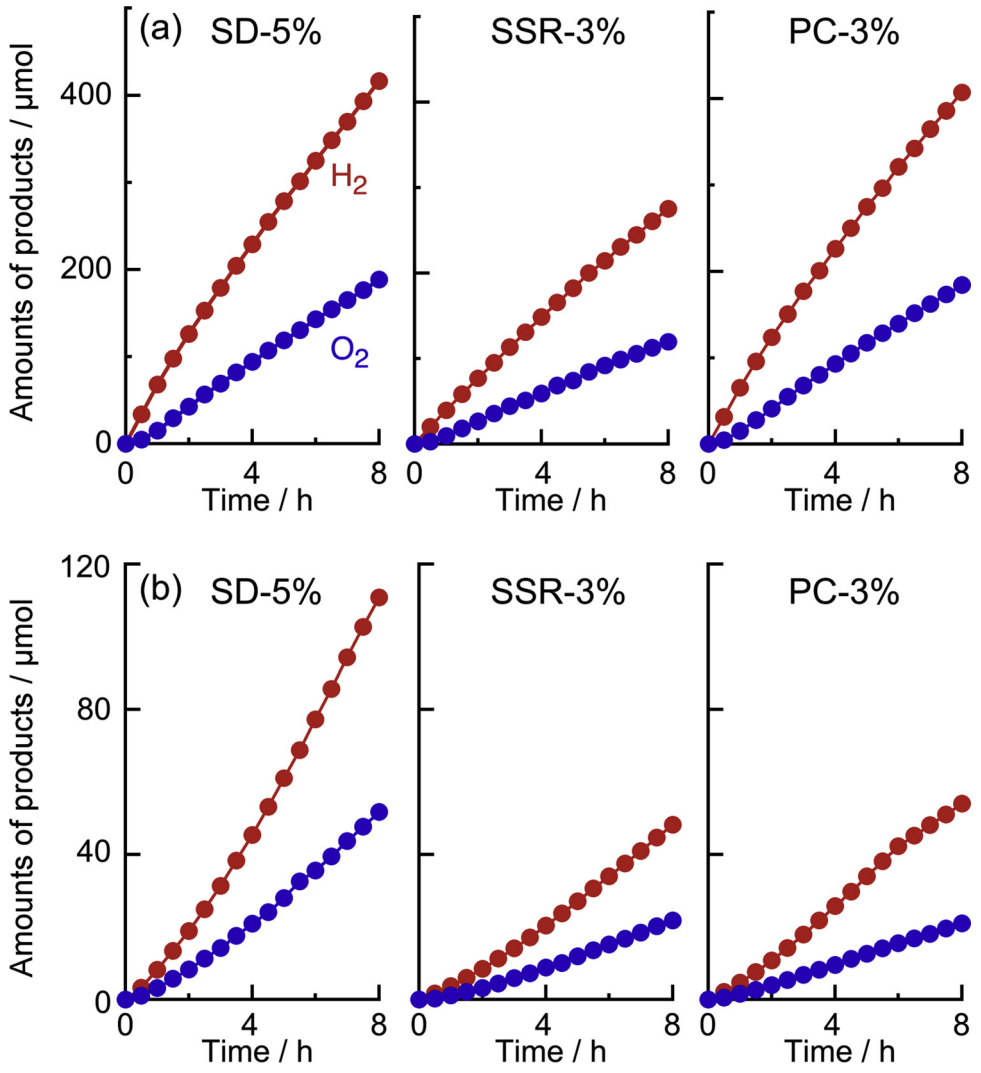

Fig. 8. Water splitting by Z-scheme systems composed of (a) Ru(1 wt%)/$SrTiO_3$:Rh, $BiVO_4$ and $[Co(bpy)_3]^{3+/2+}$ and (b) Ru(1 wt%)/$SrTiO_3$:Rh and RGO/$BiVO_4$. Catalysts: 50 mg for each, reactant solution: 160 mL of 0.5 mM $[Co(bpy)_3]SO_4$ (pH 3.8) for (a) and 160 mL of H_2SO_4 aqueous solution (pH 3.5) for (b), light source: 300 W Xe lamp ($\lambda > 420$ nm).

and SSR-3% suppressed O_2 evolution significantly whereas the inhibition of O_2 evolution by PC-3% was remarkably smaller. Thus, in addition to DLS analysis, it has been confirmed from these photocatalytic tests that SD-5% having well-dispersive nature inhibits photoexcitation of $BiVO_4$ remarkably in comparison with PC-3% with the poor dispersibility. In other words, photoexcitation of PC-3% is rather inhibited by $BiVO_4$. Therefore, the decrease in the activity for water splitting with 30 mg of PC-3% is due to further suppression of H_2 evolution over Ru/$SrTiO_3$:Rh by photo-shield with $BiVO_4$. On the other hand, the decrease in the activity of the SSR-3% system is due to low activity of SSR-3% for H_2 evolution using Fe^{2+}. It is known that efficiency for H_2 evolution basically limits overall activity of the Z-scheme system employing SSR samples [9,15]. Therefore, lowering ability for H_2 evolution with smaller amount of SSR-3% decreases the overall activity of the Z-scheme system. In contrast to the PC and SSR samples, when 50 mg of SD-5% is used for the Z-scheme, well-dispersive and highly active SD-5% provides sufficient H_2 evolution while well-dispersed SD-5% particles remarkably inhibit photoexcitation of $BiVO_4$. Even when the amount of SD-5% is reduced to 30 mg, the efficiency of H_2 evolution is still sufficient to consume Fe^{2+} produced by $BiVO_4$; meanwhile efficiency of O_2 evolution over $BiVO_4$ is increased with less photo-shield by Ru/$SrTiO_3$:Rh particles. Thus, the overall activity of the Z-scheme water splitting can be improved by well-dispersive and highly active SD-5%. However, an excessively small amount of SD-5% (20 mg) decreased activity due to insufficient efficiency of H_2 evolution. As described above, the well-dispersive nature of the SD sample brings an advantage of saving the amount of Ru/$SrTiO_3$:Rh. To confirm the advantage of the SD method to obtain well-dispersive $SrTiO_3$:Rh with high activity, pulverization of the PC sample by ball-mill treatment was examined. The large agglomerates in PC-3% were pulverized into small particles by the ball-mill treatment, resulting in improved dispersibility as shown in Fig. S8. However, such pulverization treatment remarkably decreased activities of PC-3% for both H_2 evolution and Z-scheme water splitting because of lowering crystallinity (Fig. S9). Thus, the pulverization can improve dispersibility of the PC sample; however, it is not efficient way to obtain high activity for Z-scheme water splitting.

The AQY and STH of the present SD-5% system were determined to be 3% at 420 nm and 0.07% under simulated sunlight, respectively. These values are smaller than values reported for the PC sample (4.2% of AQY and 0.1% of STH) [15]. It would be due to the slightly lower activity of $BiVO_4$ used in this research.

3.3. Utilization of SD samples for Z-scheme systems using $[Co(bpy)_3]^{3+/2+}$ or RGO/$BiVO_4$

As described above, it has been revealed that the SD samples have

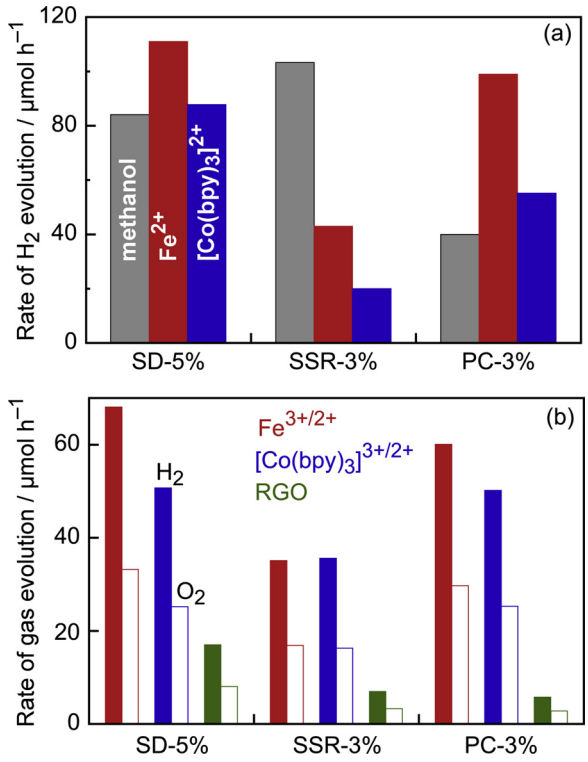

Fig. 9. Photocatalytic activities of SD-5%, SSR-3%, and PC-5% for (a) H_2 evolution using methanol, Fe^{2+}, and $[Co(bpy)_3]^{2+}$ and (b) water splitting by Z-scheme systems composed of Ru(1 wt%)/$SrTiO_3$:Rh and $BiVO_4$ using $Fe^{3+/2+}$, $[Co(bpy)_3]^{3+/2+}$, and RGO.

well-dispersive nature and high activity for H_2 evolution using Fe^{2+}. This result encouraged investigating into application of the SD samples to other Z-scheme systems. Fig. 8 shows reaction time courses of water splitting by Z-scheme systems based on the combination of Ru/$SrTiO_3$:Rh and $BiVO_4$ photocatalysts with a $[Co(bpy)_3]^{3+/2+}$ electron shuttle or RGO/$BiVO_4$. SD-5% and PC-3% showed comparable activity for water splitting using $[Co(bpy)_3]^{3+/2+}$ to each other and higher activity than SSR-3%. Higher activities for water splitting using SD-5% and PC-3% are caused by their higher activities for H_2 evolution using $[Co(bpy)_3]^{2+}$ as an electron donor as shown in Fig. S10. The similar activity between SD-5% and PC-3% for water splitting seems to be somewhat strange in consideration of 60% higher activity of SD-5% for H_2 evolution using $[Co(bpy)_3]^{2+}$ than PC-3%. It can be explained by the poor ability of $BiVO_4$ for O_2 evolution using $[Co(bpy)_3]^{3+}$ owing to competitive oxidation of $[Co(bpy)_3]^{2+}$ [16]. It means that O_2 evolution over $BiVO_4$ is being a rate determining step in the Z-scheme system with $[Co(bpy)_3]^{3+/2+}$. SD-5% also achieved overall water splitting in the interparticle electron transfer system using RGO/$BiVO_4$. For all samples, the steady activity was obtained after an induction period, which was due to photoreduction of insufficiently reduced RGO in RGO/$BiVO_4$ [14]. The order of activity for Z-scheme water splitting using RGO/$BiVO_4$ was PC-3% < SSR-3% < SD-5%.

Fig. 9 summarizes photocatalytic activities of SD-5%, SSR-3%, and PC-3% for H_2 evolution using electron donors and Z-scheme water splitting. Although SSR-3% possesses superior ability for H_2 evolution using methanol while its activities for H_2 evolution using reversible electron donors, Fe^{2+} and $[Co(bpy)_3]^{2+}$, are much lower than those of SD-5% and PC-3%. The XPS analysis revealed that SSR-3% has remarkably high concentration of Rh at surface, 9 atom% to (Ti + Rh) for 1 atom% of the nominal concentration, in comparison with the SD and PC samples as shown in Table 3. This result leads a presumption that the surface of SSR-3% with high concentration of Rh may provide highly active sites for oxidation of methanol. In contrast, SD-5% has the highest activities for all reactions except for the H_2 evolution using methanol and PC-3% has the tendency to possess the slightly lower activity than SD-5% for Z-scheme water splitting using electron shuttles. High homogeneity of constituent elements in SD-5% and PC-3%, which are derived from atomically homogeneous mixing in the solution-based processes, would positively affect photocatalytic performance like as the decreases in the number of recombination centers formed by defects including inhomogeneous local composition. It results in basically higher activities of the SD and PC samples in many kinds of reactions than the SSR sample. However, the poor dispersibility of PC-3% resulted in the lowest activity for Z-scheme water splitting using RGO because the poor-dispersive particles inefficiently create the opportunity for contact between Ru/$SrTiO_3$:Rh and RGO/$BiVO_4$, which is crucial to establish the interparticle electron transfer.

4. Conclusions

The preparation of well-dispersive and highly active $SrTiO_3$:Rh photocatalysts has been achieved by a SD method employing water-soluble trilactatotitanate complex. The SD sample has much higher activities than the SSR sample for H_2 evolution and Z-scheme water splitting using reversible redox species, $Fe^{3+/2+}$ and $[Co(bpy)_3]^{3+/2+}$ like as the PC sample. However, the SD sample has a superior feature to the PC sample, well-dispersibility. The well-dispersive nature of the SD sample enables to reduce the mass of $SrTiO_3$:Rh in Z-scheme systems and causes high activity in Z-scheme water splitting with interparticle electron transfer due to frequent contact between Ru/$SrTiO_3$:Rh and RGO/$BiVO_4$. Thus, the present study has firstly demonstrated improvements of Z-scheme systems with $[Co(bpy)_3]^{3+/2+}$ by the SD and PC samples and the system with RGO by the SD sample. The high activity for H_2 evolution using $[Co(bpy)_3]^{2+}$ is an interesting characteristic of the SD sample. The Z-scheme system with $[Co(bpy)_3]^{3+/2+}$ has the advantage of availability in wide pH of the reaction condition in comparison with the $Fe^{3+/2+}$-system requiring acidic condition, pH < 2.5. Although the present activity of the SD sample for Z-scheme water splitting using $[Co(bpy)_3]^{3+/2+}$ is almost the same as that of the PC sample due to low efficiency of O_2 evolution over $BiVO_4$, the higher activity of the SD sample for H_2 evolution suggests the possibility of further improvement of efficiency in Z-scheme water splitting using $[Co(bpy)_3]^{3+/2+}$ by highly efficient O_2-evolving photocatalysts.

Acknowledgements

This research was partly supported by Japan Society for the Promotion of Science KAKENHI (Grant Number JP16H04186), Joint Usage/Research Center Program of “Photocatalysis International Research Center” at Tokyo University of Science, and “Dynamic Alliance for Open Innovation Bridging Human, Environment and Materials” in “Network Joint Research Center for Materials and Devices”

Appendix A. Supplementary data

Supplementary material related to this article can be found, in the online version, at doi:https://doi.org/10.1016/j.apcatb.2019.04.009.

References

[1] N.S. Lewis, Research opportunities to advance solar energy utilization, Science 351 (2016), https://doi.org/10.1126/science.aad1920 aad1920.
[2] A. Kudo, Y. Miseki, Heterogeneous photocatalyst materials for water splitting, Chem. Soc. Rev. 38 (2009) 253–278, https://doi.org/10.1039/b800489g.
[3] Y.P. Yuan, L.W. Ruan, J. Barber, S.C.J. Loo, C. Xue, Hetero-nanostructured suspended photocatalysts for solar-to-fuel conversion, Energy Environ. Sci. 7 (2014) 3934–3951, https://doi.org/10.1039/C4EE02914C.
[4] Y. Ma, X. Wang, Y. Jia, X. Chen, H. Han, C. Li, Titanium dioxide-based nanomaterials for photocatalytic fuel generations, Chem. Rev. 114 (2014) 9987–10043, https://doi.org/10.1021/cr500008u.

[5] D.M. Fabian, S. Hu, N. Singh, F.A. Houle, T. Hisatomi, K. Domen, F.E. Osterloh, S. Ardo, Particle suspension reactors and materials for solar-driven water splitting, Energy Environ. Sci. 8 (2015) 2825–2850, https://doi.org/10.1039/C5EE01434D.

[6] H. Yi, D. Huang, L. Qin, G. Zeng, C. Lai, M. Cheng, S. Ye, B. Song, X. Ren, X. Guo, Selective prepared carbon nanomaterials for advanced photocatalytic application in environmental pollutant treatment and hydrogen production, Appl. Catal. B Environ. 239 (2018) 408–424, https://doi.org/10.1016/j.apcatb.2018.07.068.

[7] Y. Yang, C. Zhang, D. Huang, G. Zeng, J. Huang, C. Lai, C. Zhou, W. Wang, H. Guo, W. Xue, R. Deng, M. Cheng, W. Xiong, Boron nitride quantum dots decorated ultrathin porous g-C_3N_4 : intensified exciton dissociation and charge transfer for promoting visible-light-driven molecular oxygen activation, Appl. Catal. B Environ. 245 (2019) 87–99, https://doi.org/10.1016/j.apcatb.2018.12.049.

[8] H. Yi, L. Qin, D. Huang, G. Zeng, C. Lai, X. Liu, B. Li, H. Wang, C. Zhou, F. Huang, S. Liu, X. Guo, Nano-structured bismuth tungstate with controlled morphology: fabrication, modification, environmental application and mechanism insight, Chem. Eng. J. 358 (2019) 480–496, https://doi.org/10.1016/j.cej.2018.10.036.

[9] H. Kato, M. Hori, R. Konta, Y. Shimodaira, A. Kudo, Construction of Z-scheme type heterogeneous photocatalysis systems for water splitting into H_2 and O_2 under visible light irradiation, Chem. Lett. 33 (2004) 1348–1349, https://doi.org/10.1246/cl.2004.1348.

[10] H. Kato, Y. Sasaki, A. Iwase, A. Kudo, Role of iron ion electron mediator on photocatalytic overall water splitting under visible light irradiation using Z-Scheme systems, Bull. Chem. Soc. Jpn. 80 (2007) 2457–2464, https://doi.org/10.1246/bcsj.80.2457.

[11] M. Higashi, R. Abe, K. Teramura, T. Takata, B. Ohtani, K. Domen, Two step water splitting into H_2 and O_2 under visible light by $ATaO_2N$ (A = Ca, Sr, Ba) and WO_3 with IO_3^-/I^- shuttle electron mediator, Chem. Phys. Lett. 452 (2008) 120–123, https://doi.org/10.1016/j.cplett.2007.12.021.

[12] Y. Sasaki, H. Nemoto, K. Saito, A. Kudo, Solar water splitting using powdered photocatalysts driven by Z-schematic interparticle electron transfer without an electron mediator, J. Phys. Chem. C 113 (2009) 17536–17542, https://doi.org/10.1021/jp907128k.

[13] Y. Sasaki, A. Iwase, H. Kato, A. Kudo, The effect of co-catalyst for Z-scheme photocatalysis systems with an Fe^{3+}/Fe^{2+} electron mediator on overall water splitting under visible light irradiation, J. Catal. 259 (2008) 133–137, https://doi.org/10.1016/j.jcat.2008.07.017.

[14] A. Iwase, Y.H. Ng, Y. Ishiguro, A. Kudo, R. Amal, Reduced graphene oxide as a solid-state electron mediator in Z-Scheme photocatalytic water splitting under visible light, J. Am. Chem. Soc. 133 (2011) 11054–11057, https://doi.org/10.1021/ja203296z.

[15] H. Kato, Y. Sasaki, N. Shirakura, A. Kudo, Synthesis of highly active rhodium-doped $SrTiO_3$ powders in Z-scheme systems for visible-light-driven photocatalytic overall water splitting, J. Mater. Chem. A 1 (2013) 12327–12333, https://doi.org/10.1039/C3TA123803B.

[16] Y. Sasaki, H. Kato, A. Kudo, $[Co(bpy)_3]^{3+/2+}$ and $[Co(phen)_3]^{3+/2+}$ electron mediators for overall water splitting under sunlight irradiation using Z-scheme photocatalyst system, J. Am. Chem. Soc. 135 (2013) 5441–5449, https://doi.org/10.1021/ja400238r.

[17] K. Maeda, Z-scheme water splitting using two different semiconductor photocatalysts, ACS Catal. 3 (2013) 1486–1503, https://doi.org/10.1021/cs4002089.

[18] W. Wang, J. Chen, C. Li, W. Tian, Achieving solar overall water splitting with hybrid photosystems of photosystem II and artificial photocatalysts, Nat. Commun. 5 (2014) 1–8, https://doi.org/10.1038/ncomms5647.

[19] Q. Jia, A. Iwase, A. Kudo, $BiVO_4$–Ru/$SrTiO_3$:Rh composite Z-scheme photocatalyst for solar water splitting, Chem. Sci. 5 (2014) 1513–1519, https://doi.org/10.1039/C3SC52810C.

[20] R. Niishiro, S. Tanaka, A. Kudo, Hydrothermal-synthesized $SrTiO_3$ photocatalyst codoped with rhodium and antimony with visible-light response for sacrificial H_2 and O_2 evolution and application to overall water splitting, Appl. Catal. B Environ. 150–151 (2014) 187–196, https://doi.org/10.1016/j.apcatb.2013.12.015.

[21] K. Iwashina, A. Iwase, Y.H. Ng, R. Amal, A. Kudo, Z-schematic water splitting into H_2 and O_2 using metal sulfide as a hydrogen-evolving photocatalyst and reduced graphene oxide as a solid-state electron mediator, J. Am. Chem. Soc. 137 (2015) 604–607, https://doi.org/10.1021/ja511615s.

[22] Q. Wang, T. Hisatomi, Q. Jia, H. Tokudome, M. Zhong, C. Wang, Z. Pan, T. Takata, M. Nakabayashi, N. Shibata, Y. Li, I.D. Sharp, A. Kudo, T. Yamada, K. Domen, Scalable water splitting on particulate photocatalyst sheets with a solar-to-hydrogen energy conversion efficiency exceeding 1%, Nat. Mater. 15 (2016) 611–615, https://doi.org/10.1038/nmat4589.

[23] H. Suzuki, S. Nitta, O. Tomita, M. Higashi, R. Abe, Highly dispersed RuO_2 hydrates prepared *via* simple adsorption as efficient cocatalysts for visible-light-driven Z-scheme water splitting with an IO_3^-/I^- redox mediator, ACS Catal. 7 (2017) 4336–4343, https://doi.org/10.1021/acscatal.7b00953.

[24] T. Shirakawa, M. Higashi, O. Tomita, R. Abe, Surface-modified metal sulfides as stable H_2-evolving photocatalysts in Z-scheme water splitting with a $[Fe(CN)_6]^{3-/4-}$ redox mediator under visible-light irradiation, Sustain. Energy Fuels 1 (2017) 1065–1073, https://doi.org/10.1039/C7SE00151G.

[25] A. Rauf, M. Ma, S. Kim, M.S.A.S. Shah, C.H. Chung, J.H. Park, P.J. Yoo, Mediator- and co-catalyst-free direct Z-scheme composites of Bi_2WO_6–Cu_3P for solar-water splitting, Nanoscale 10 (2018) 3026–3036, https://doi.org/10.1039/C7NR07952D.

[26] Y. Wang, H. Suzuki, J. Xie, O. Tomita, D.J. Martin, M. Higashi, D. Kong, R. Abe, J. Tang, Mimicking natural photosynthesis: solar to renewable H_2 fuel synthesis by Z-scheme water splitting systems, Chem. Rev. 118 (2018) 5201–5241, https://doi.org/10.1021/acs.chemrev.7b00286.

[27] Y. Miseki, K. Sayama, Photocatalytic water splitting for solar hydrogen production using the carbonate effect and the Z-scheme reaction, Adv. Energy Mater. (2018) 1801294, , https://doi.org/10.1002/aenm.201801294.

[28] R. Konta, T. Ishii, H. Kato, A. Kudo, Photocatalytic activities of noble metal ion doped $SrTiO_3$ under visible light irradiation, J. Phys. Chem. B 108 (2004) 8992–8995, https://doi.org/10.1021/jp049556p.

[29] S. Okunaka, H. Tokudome, R. Abe, Facile water-based preparation of Rh-doped $SrTiO_3$ nanoparticles for efficient photocatalytic H_2 evolution under visible light irradiation, J. Mater. Chem. A 3 (2015) 14794–14800, https://doi.org/10.1039/C5TA02903A.

[30] T. Murakata, R. Yamamoto, Y. Yoshida, M. Hinihara, T. Ogata, S. Sato, Preparation of ultra fine TiO_2 particles dispersible in organic solvents and their photocatalytic properties, J. Chem. Eng. Jpn. 31 (1998) 21–28, https://doi.org/10.1252/jcej.31.21.

[31] Y. Xu, W. Zheng, W. Liu, Enhanced photocatalytic activity of supported TiO_2: dispersing effect of SiO_2, J. Photochem. Photobiol. A Chem. 122 (1999) 57–60, https://doi.org/10.1016/S1010-6030(98)00470-5.

[32] T.A. Egerton, I.R. Tooley, Effect of changes in TiO_2 dispersion on its measured photocatalytic activity, J. Phys. Chem. B 108 (2004) 5066–5072, https://doi.org/10.1021/jp0378992.

[33] B. Faure, J.S. Lindelov, M. Wahlberg, M. Adkins, P. Jackson, L. Bergstrom, Spray drying of TiO_2 nanoparticles into redispersible granules, Powder Technol. 203 (2010) 384–388, https://doi.org/10.1016/j.powtec.2010.05.033.

[34] B. Mei, M.D. Sánchez, T. Reinecke, S. Kaluza, W. Xia, M. Muhler, The synthesis of Nb-doped TiO_2 nanoparticles by spray drying: an efficient and scalable method, J. Mater. Chem. 21 (2011) 11781–11790, https://doi.org/10.1039/C1JM11431J.

[35] S.I. Cha, B.K. Koo, K.H. Hwang, S.H. Seo, D.Y. Lee, Spray-dried and pre-sintered TiO_2 micro-balls for sinter-free processing of dye-sensitized solar cells, J. Mater. Chem. 21 (2011) 6300–6304, https://doi.org/10.1039/C0JM04450D.

[36] S. Pal, A.M. Laera, A. Licciculli, M. Catalano, A. Taurino, Biphase TiO_2 microspheres with enhanced photocatalytic activity, Ind. Eng. Chem. Res. 53 (2014) 7931–7938, https://doi.org/10.1021/ie404123f.

[37] M. Kakihana, K. Tomita, V. Petrykin, M. Tada, S. Sasaki, Y. Nakamura, Chelating of titanium by lactic acid in the water-soluble diammonium tris(2-hydroxypropionato) titanate(IV), Inorg. Chem. 43 (2004) 4546–4548, https://doi.org/10.1021/ic040031l.

[38] K. Tomita, V. Petrykin, M. Kobayashi, M. Shiro, M. Yoshimura, M. Kakihana, A Water-Soluble titanium complex for the selective synthesis of nanocrystalline brookite, rutile, and anatase by a hydrothermal method, Angew. Chem. Int. Ed. 45 (2006) 2378–2381, https://doi.org/10.1002/anie.200503565.

[39] M. Kakihana, M. Kobayashi, K. Tomita, V. Petrykin, Application of water-soluble titanium complexes as precursors for synthesis of titanium-containing oxides via aqueous solution processes, Bull. Chem. Soc. Jpn. 83 (2010) 1285–1308, https://doi.org/10.1246/bcsj.20100103.

[40] A. Kudo, K. Omori, H. Kato, A novel aqueous process for preparation of crystal form-controlled and highly crystalline $BiVO_4$ powder from layered vanadates at room temperature and and its photocatalytic and photophysical properties, J. Am. Chem. Soc. 121 (1999) 11459–11467, https://doi.org/10.1021/ja992541y.

[41] H. Kato, K. Shimizu, K. Nakajima, M. Kobayashi, M. Kakihana, Synthesis of rare earth niobates and tantalates powders via a peroxo complex route, Chem. Lett. 46 (2017) 1515–1517, https://doi.org/10.1246/cl.170652.